2016 American Control Conference (ACC)
Boston Marriott Copley Place
July 6-8, 2016. Boston, MA, USA

Model-based Sensor Fault Diagnostics of Double-Layer Capacitors

Satadru Dey, *Member, IEEE*, Sara Mohon, *Member, IEEE,* Simona Onori, *Senior Member, IEEE*

***Abstract*—Double-Layer Capacitors (DLC) are becoming popular energy storage elements in several systems such as automotive propulsion systems, renewable energy storage and auxiliary power units. Optimal energy management, estimation and control algorithms for such DLCs heavily depend on sensor measurements, namely voltage, current and temperature sensors. Any fault in such sensors may result in degraded operation of DLCs thereby increasing the risk of significant damage. In this paper, an equivalent circuit model in conjunction with a set of observers is employed to design a sensor fault diagnosis scheme for DLCs. The scheme consists of an electrical and a temperature observer, the output errors of which are used as residual signals for fault diagnosis. Further, to suppress the effects of modeling uncertainties, adaptive threshold generators are also designed. Simulation studies are presented to validate the effectiveness of the proposed approach.**

I. Introduction

The Double Layer Capacitor has become a popular alternative energy storage choice for many applications, such as automotive, wind turbine, circuit power protection, and aviation [1, 2]. The main attraction of DLC is its long cycle life and high power density and can be utilized to assist other energy storage elements during high current situations thus reducing the aging and fatigue of the main energy storage element, e.g. batteries [3].

The dependence of DLC on operating conditions can cause these devices to undergo severe aging processes [4]. Tracking the aging process is necessary for health monitoring and optimal management of DLCs [3,5]. Among different modeling approaches, the equivalent circuit model (ECM) is widely used due to its simplified structure and computational efficiency. The parameters of ECM are useful indicators of DLC state of health (SOH) [6]. There exist a few approaches that explore the estimation problem for DLCs. For example, Extended Kalman Filters (EKF) for state estimation [3,7], least squares method for parameter estimation [8,9], a dual Kalman filter for combined state and parameter estimation [5], sliding mode observer based approach for combined state and parameter estimation [10].

Unlike the estimation problem, fault diagnosis of DLCs is an underexplored topic in existing literature. Of the existing literature, fault modes are typically categorized into end-of-life categories that are correlated with Equivalent Series Resistance (ESR) and capacitance values of the DLC [11-13]. In [12, 13] the ESR and capacitance values are calculated using the least squares algorithm and current and voltage measurements. In [14], over-voltage or over-temperature faults are correlated to ESR or capacitance values. However, none of these existing works explore the problem of sensor fault diagnosis in DLCs.

Sensor faults can have significant implications on safe DLC operation. The feedback-based estimation and optimal management algorithm for DLCs generally rely on voltage, temperature and current sensor measurements. In this work, we propose a model-based sensor fault diagnosis approach using an equivalent circuit model due to its computational efficiency and ability to predict output with significant accuracy. The diagnostic algorithm uses an observer-based method which is widely used in model-based fault diagnosis [15]. The diagnostic scheme consists of two observers, electrical and temperature. The output estimation errors of these observers are used as residual signals for fault diagnosis. We apply the adaptive thresholding approach to deal with uncertainties [16]. The adaptive threshold generator is essentially a dynamic filter that generates a threshold value based on the known bounds of modeling uncertainties. A fault occurs when the residual goes beyond the adaptive threshold.

The rest of the paper is organized as follows. Section II discusses the modeling approach for the DLC. Section III outlines the diagnostic scheme with observer design and adaptive threshold design. Section IV presents simulation studies to validate the effectiveness of the approach. Section V concludes this work.

II. Modeling of Double-Layer Capacitors

The equivalent electrical circuit used to model the DLC in this paper is shown in Fig.1 with two resistor-capacitor branches in parallel where R_f and R_d are the resistances and C_f and C_d are the capacitances [17]. Note that, the $R_d - C_d$ branch represents the slow dynamics of the system with higher resistance and capacitance whereas the $R_f - C_f$ branch represents the fast dynamics of the system with lower resistance and capacitance.

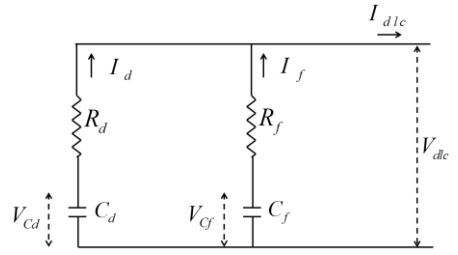

Figure 1: Electrical equivalent circuit model of DLC

Across the capacitors, the voltage dynamics will be:

$$\dot{V}_{cf} = \frac{I_f}{C_f} \tag{1}$$

S. Dey is with Department of Civil and Environmental Engineering, University of California, Berkeley. S. Onori is with Department of Automotive Engineering, Clemson University, SC 29607 USA (e-mail: satadru86@berkeley.edu, smohon@g.clemson.edu, sonori@clemson.edu). S. Dey and S. Mohon were with Department of Automotive Engineering, Clemson University at the time of this research.

$$\dot{V}_{cd} = \frac{I_d}{C_d} \tag{2}$$

where V_{cf} is the voltage across capacitor C_f, V_{cd} is the voltage across capacitor C_d, I_d is the current flowing through the $R_d - C_d$ branch, I_f is the current flowing through the $R_f - C_f$ branch. Kirchoff's current law gives the total current I_{dlc} entering the DLC as:

$$I_{dlc} = I_f + I_d \tag{3}$$

and the effective total voltage V_{dlc} across the DLC is:

$$V_{dlc} = I_f R_f + V_{cf} = I_d R_d + V_{cd} \tag{4}$$

Here, positive current indicates discharge. In this model, a lumped thermal dynamics model is used [17]. We follow the convention of positive current indicates discharge. The lumped thermal dynamics of the DLC is given by:

$$mc\dot{T} = I_{dlc}^2 R_f - hA(T - T_{amb}) \tag{5}$$

where T is the DLC temperature, mc is the mass multiplied by the specific heat capacity of the DLC, and hA is the effective heat transfer coefficient. The heat generated in (5) is not a function of R_d because the current through R_d is negligible when compared to the current through R_f [17].

It is worth mentioning that the DLC model parameters R_f, R_d, C_f and C_d may depend on the SOC, temperature and current. However, experimental data from literature and DLC manufacturer datasheets show that these parameters are primarily functions of temperature [17, 19].

III. Diagnostic Scheme

In this section, we will discuss the diagnostic scheme in detail. As mentioned before, the main objective of this scheme is to detect and isolate the faults in the sensors of DLC, namely the voltage, temperature and current sensor. From the depiction of the scheme in Fig. 2, it can be noted that it consists of two parts: residual generation via the electrical and temperature observer and adaptive threshold generation to suppress the effect of uncertainties. Thereafter, the residuals are compared to the adaptive thresholds in the residual evaluation stage. The details of the design of these individual elements are discussed in the subsequent sections. In the following analysis, we will use I_{dlc_m}, V_{dlc_m} and T_m to denote measured current, voltage and temperature.

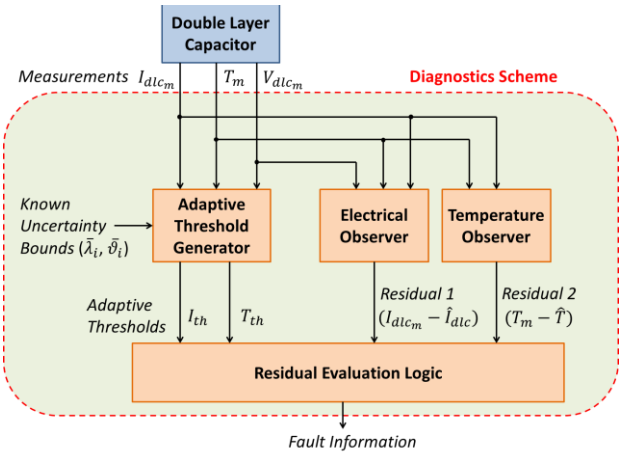

Figure 2: Diagnostic scheme

A. Observer Design for Primary Residual Generation

Note that, the structure of the DLC model given in (1)-(4) is complex for observer design as the individual inputs to the state dynamics (i.e. I_f and I_d) are not known. To overcome this issue, we reduce the model complexity by reformulating (1)-(4). Taking the time-derivative on the both sides of the first equation of (4), we have:

$$\begin{aligned} &\dot{V}_{dlc} = \dot{I}_f R_f(T) + I_f \dot{R}_f(T) + \dot{V}_{cf} \\ &\Rightarrow \dot{V}_{dlc} = \dot{I}_f R_f(T) + I_f \frac{\partial R_f}{\partial T}\dot{T} + \dot{V}_{cf} \end{aligned} \tag{6}$$

Now, using (1), (6) can be written as:

$$\dot{V}_{dlc} = \dot{I}_f R_f(T) + I_f \frac{\partial R_f}{\partial T}\dot{T} + \frac{I_f}{C_f(T)} \tag{7}$$

Note that, the electrical time constant (in order of seconds) is much faster than the thermal time constant (in order of hour), which justifies the term $\dot{T}$ to be neglected and approximated as zero making (7) as:

$$\dot{I}_f = -\frac{I_f}{R_f(T)C_f(T)} + \frac{\dot{V}_{dlc}}{R_f(T)} \tag{8}$$

Following similar steps, based on the second equation of (4), the state dynamics for I_d can be written as:

$$\dot{I}_d = -\frac{I_d}{R_d(T)C_d(T)} + \frac{\dot{V}_{dlc}}{R_d(T)} \tag{9}$$

Note that, the input excitation in (8) and (9) is $\dot{V}_{dlc}$ which is not measured, however, V_{dlc} is a measured variable. To avoid the direct differentiation of the measured variable, we apply the following filtering mechanism [18]:

$$\begin{aligned} &\dot{z} = -\frac{z}{\tau_f} + V_{dlc} \\ &u = -z + \frac{V_{dlc}}{\tau_f} \end{aligned} \tag{10}$$

where z is an intermediate auxiliary variable, τ_f is the filter time constant and the filter output u can be substituted in place of $\dot{V}_{dlc}$ while implementing (8)-(9). Note that, the choice of τ_f should be made under the trade-off of measurement noise amplification and filter convergence rate. Therefore, the reformulated electrical dynamics can be written as:

$$\begin{aligned} \dot{I}_f &= -\frac{I_f}{R_f(T)C_f(T)} + \frac{u}{R_f(T)} \\ \dot{I}_d &= -\frac{I_d}{R_d(T)C_d(T)} + \frac{u}{R_d(T)} \end{aligned} \tag{11}$$

The measured output of the above system is the total DLC current $I_{dlc_m} = I_f + I_d$. Now, we discuss the observer design process for the residual generation. Based on the system model (11) and output error injection, the following electrical observer structure is chosen as:

$$\dot{\hat{I}}_f = -\frac{\hat{I}_f}{R_f(T_m)C_f(T_m)} + \frac{u}{R_f(T_m)} + L_f(T_m)(I_{dlc_m} - \hat{I}_{dlc})$$
$$\dot{\hat{I}}_d = -\frac{\hat{I}_d}{R_d(T_m)C_d(T_m)} + \frac{u}{R_d(T_m)} + L_d(T_m)(I_{dlc_m} - \hat{I}_{dlc}) \quad (12)$$

where T_m is the measured temperature, $\hat{I}_f$ and $\hat{I}_d$ are the estimated branch currents, $\hat{I}_{dlc} = \hat{I}_f + \hat{I}_d$ is the estimated output, L_f and L_d are observer gains that are scheduled as functions of temperature. Subtracting (12) from (11), the nominal estimation error dynamics (i.e. without any sensor fault) can be written as:

$$\begin{bmatrix}\dot{\tilde{I}}_f \\ \dot{\tilde{I}}_d\end{bmatrix} = \begin{bmatrix}a_{11} & a_{12} \\ a_{21} & a_{22}\end{bmatrix}\begin{bmatrix}\tilde{I}_f \\ \tilde{I}_d\end{bmatrix}$$
$$\text{with} \quad a_{11} = -\frac{1}{R_f(T_m)C_f(T_m)} - L_f(T), a_{12} = -L_f(T),$$
$$a_{21} = -L_d(T), a_{22} = -\frac{1}{R_d(T)C_d(T)} - L_d(T) \quad (13)$$

where $\tilde{I}_f = I_f - \hat{I}_f$, $\tilde{I}_d = I_d - \hat{I}_d$. The positive observer gains L_f and L_d can be determined offline over an temperature operating range ($T \in [T_{min}, T_{max}]$) to ensure that the closed-loop matrix $[a_{11}, a_{12}; a_{21}, a_{22}]$ is Hurwitz stable, i. e., all the poles have strictly negative real parts for each temperature operating point (T^*). In real-time implementation, these pre-determined gains can be fed to the observer as a function of temperature. By this selection of gains, the estimation errors $\tilde{I}_d, \tilde{I}_f \to 0$ as $t \to \infty$. Now, we define the first residual, $Residual\ 1 = (I_{dlc_m} - \hat{I}_{dlc})$. Therefore, if there is no fault, the $Residual\ 1$ which is $\tilde{I}_{dlc}$ in this case, goes to zero asymptotically.

Similarly, the temperature observer structure is chosen as:

$$mc\dot{\hat{T}} = -hA\left(\hat{T} - T_{amb}\right) + I_{dlc_m}^2 R_f(T_m) + L_T(T_m - \hat{T}) \quad (14)$$

where L_T is the observer gain to be designed. Subtracting (15) and (14), the nominal estimation error dynamics (without any sensor fault) can be written as:

$$mc\dot{\tilde{T}} = -hA\tilde{T} - L_T\tilde{T} \quad (15)$$

The gain L_T can be chosen as sufficiently high positive to ensure the desired convergence rate of the estimation error. Now, we define the second residual $Residual\ 2 = T_m - \hat{T}$. If there is no fault, the $Residual\ 2$ which is $\tilde{T}$ in this case, goes to zero asymptotically.

In the previous analysis, it is proved that the residuals are zero in presence of no faults. Now, we analyze the effects of the individual sensor faults on the residuals.

Case 1, Voltage sensor fault: In case of voltage sensor fault, Δ_V, we have $V_{dlc_m} = V_{dlc} + \Delta_V$. Therefore, the electrical observer error dynamics becomes:

$$\begin{bmatrix}\dot{\tilde{I}}_f \\ \dot{\tilde{I}}_d\end{bmatrix} = \begin{bmatrix}a_{11} & a_{12} \\ a_{21} & a_{22}\end{bmatrix}\begin{bmatrix}\tilde{I}_f \\ \tilde{I}_d\end{bmatrix} + \begin{bmatrix}\frac{\dot{\Delta}_V}{R_f(T)} \\ \frac{\dot{\Delta}_V}{R_d(T)}\end{bmatrix} \quad (16)$$

From (16), one can see that the state estimation errors Id and If (hence Residual 1) are being driven $\dot{\Delta}_V$ and will be nonzero as long as $\dot{\Delta}_V \neq 0$. However, in this fault case, the $Residual\ 2$ will be zero as the voltage does not affect the thermal dynamics.

Case 2, Current sensor fault: In case of current sensor fault, we have $I_{dlc_m} = I_{dlc} + \Delta_I$ where Δ_I is the sensor fault. Therefore, the electrical observer error dynamics becomes:

$$\begin{bmatrix}\dot{\tilde{I}}_f \\ \dot{\tilde{I}}_d\end{bmatrix} = \begin{bmatrix}a_{11} & a_{12} \\ a_{21} & a_{22}\end{bmatrix}\begin{bmatrix}\tilde{I}_f \\ \tilde{I}_d\end{bmatrix} + \begin{bmatrix}L_f(T_m)\Delta_I \\ L_d(T_m)\Delta_I\end{bmatrix} \quad (17)$$

It can be seen from the above equation that state estimation errors $\tilde{I}_d, \tilde{I}_f$ and hence $Residual\ 1$ is being driven by the fault Δ_I and hence will be non-zero if $\Delta_I \neq 0$. Further, the temperature observer error dynamics becomes:

$$mc\dot{\tilde{T}} = -hA\tilde{T} - L_T\tilde{T} + \{I_{dlc}^2 - (I_{dlc} + \Delta_I)^2\}R_f(T_m) \quad (18)$$

where it is evident that the $Residual\ 2$ will be nonzero if $\Delta_I \neq 0$.

Case 3, Temperature sensor fault: In case of temperature sensor fault, we have $T_m = T + \Delta_T$ where Δ_T is the sensor fault. Therefore, the electrical observer error dynamics becomes:

$$\begin{bmatrix}\dot{\tilde{I}}_f \\ \dot{\tilde{I}}_d\end{bmatrix} = \begin{bmatrix}a_{11} & a_{12} \\ a_{21} & a_{22}\end{bmatrix}\begin{bmatrix}\tilde{I}_f \\ \tilde{I}_d\end{bmatrix} + \begin{bmatrix}f_1(\Delta_T, \hat{I}_f, u) \\ f_2(\Delta_T, \hat{I}_d, u)\end{bmatrix} \quad (19)$$

where f_1 and f_2 are the lumped effects of Δ_T which makes $Residual\ 1$ nonzero. Similarly, the $Residual\ 2$ will be nonzero in presence of Δ_T temperature as can be seen below:

$$mc\dot{\tilde{T}} = -hA\tilde{T} - L_T\tilde{T} + I_{dlc}^2\{R_f(T) - R_f(T + \Delta_T)\} - L_T\Delta_T \quad (20)$$

Isolability of current and temperature sensor fault: It can be noted from the discussion above that both residuals will be nonzero in presence of either current or temperature sensor fault. Therefore, in general these faults may not be isolable. However, based on specific characteristics of the system and practical consideration, we can derive some isolability conditions for these two faults. Generally, the maps $R_f(.)$, $R_d(.)$, $C_f(.)$ and $C_d(.)$ have low sensitivity with respect to the temperature change (e.g. one may refer to these maps shown in [17] for a commercial DLC). Therefore, if the temperature sensor fault is not too high, the lumped fault effects f_1 and f_2 in (19) will not be significant. It is highly likely that such small effects may not be visible in the $Residual\ 1$ in presence of modeling uncertainties and measurement noise. However, in case of very large temperature sensor fault, the effect of f_1 and f_2 might be significant making current and temperature sensor faults not isolable.

Based on the above analysis, now we can derive the fault signature table as given below:

TABLE I: FAULT SIGANTURE TABLE ("1" INDICATES NONZERO, "0" INDICATES ZERO, "×" INDICATES EITHER ZERO OR NONZERO)

Residual Signals		Fault Detection/ Isolation
$Residual\ 1$ $(I_{dlc_m} - \hat{I}_{dlc})$	$Residual\ 2$ $(T_m - \hat{T})$	
1	0	Voltage Sensor
1	1	Current Sensor
×	1	Temperature Sensor

Note that, in case of temperature sensor fault, we have "×" for the $Residual\ 1$. This indicates that this residual will be zero unless of high fault magnitude.

B. Adaptive Threshold Design for Robustness to Uncertainties

In real applications, uncertainties such as modeling errors, parametric deviations, and measurement inaccuracies are always present. Therefore, the residuals will not be zero due to the presence of uncertainties even if there is no fault. To improve the robustness of the fault detection scheme, adaptive thresholds can be designed based on uncertainty bounds in the residual evaluation stage [16]. The estimation errors, which are the residuals of the detection scheme, will be compared to these adaptive thresholds to determine whether a fault has occurred. The residual evaluation logic will be: if the residual is greater than the threshold, then there is fault, otherwise no fault.

The error dynamics of the electrical observer, along with the uncertainties, can be written as:

$$\begin{bmatrix} \dot{\tilde{I}}_f \\ \dot{\tilde{I}}_d \end{bmatrix} = \begin{bmatrix} a_{11} & a_{12} \\ a_{21} & a_{22} \end{bmatrix} \begin{bmatrix} \tilde{I}_f \\ \tilde{I}_d \end{bmatrix} + \begin{bmatrix} \eta_f \\ \eta_d \end{bmatrix} \tag{21}$$

where η_f, η_d are the uncertainties and possibly nonlinear functions of states and inputs. Based on (21), the $Residual\ 1$ error dynamics under no fault can be written as:

$$\dot{\tilde{I}}_{dlc} = K_1 \tilde{I}_f + K_2 \tilde{I}_d + \eta_f + \eta_d \tag{22}$$

where $K_1 = (a_{11} + a_{21})$ and $K_2 = (a_{12} + a_{22})$. Note that, both K_1 and K_2 are negative by choice of the observer gains. The above equation can be written as:

$$\begin{aligned} &\dot{\tilde{I}}_{dlc} = K_1\left(\tilde{I}_f + \tilde{I}_d\right) + \eta \\ &\Rightarrow \dot{\tilde{I}}_{dlc} = K_{1m}\tilde{I}_{dlc} + \eta \end{aligned} \tag{23}$$

where $K_{1m} = \max(K_1)$ over the operating temperature range, $\eta = (K_1 - K_{1m})\tilde{I}_{dlc} + (K_2 - K_1)\tilde{I}_d + \eta_f + \eta_d$ is the lumped effect of uncertainties and approximation errors. Next, we approximate η as linearly parameterized with respect to the measured signals:

$$\eta \cong \lambda_1 I_{dlc} + \lambda_2 u + \lambda_3 T + \lambda_4 \tag{24}$$

where λ_i are generally time-varying, unknown but bounded coefficients and λ_4 captures all the nonlinearities and approximation errors of the linear parameterization. The known bounds of these parameters are $\lambda_i \le \bar{\lambda}_i$. The error evolution integral of (23) can be written as:

$$\begin{aligned} &\tilde{I}_{dlc}(t) = \tilde{I}_{dlc}(0)e^{K_{1m}t} + \\ &\int_0^t e^{K_{1m}(t-\tau)}\{\lambda_1(\tau)I_{dlc}(\tau) + \lambda_2(\tau)u(\tau) \\ &+ \lambda_3(\tau)T(\tau) + \lambda_4(\tau)\}d\tau \end{aligned} \tag{25}$$

Using the bounding argument $ab \le |a||b|$ on the product terms inside the integral, (25) can be written as:

$$\begin{aligned} &\tilde{I}_{dlc}(t) \le \tilde{I}_{dlc}(0)e^{K_{1m}t} + \\ &\int_0^t \{\left|e^{K_{1m}(t-\tau)}\right||\lambda_1(\tau)||I_{dlc}(\tau)| \\ &+ \left|e^{K_{1m}(t-\tau)}\right||\lambda_2(\tau)||u(\tau)| \\ &+ \left|e^{K_{1m}(t-\tau)}\right||\lambda_3(\tau)||T(\tau)| + \left|e^{K_{1m}(t-\tau)}\right||\lambda_4(\tau)|\}d\tau \end{aligned} \tag{26}$$

Note the K_{1m} is a negative scalar and therefore we have the following condition always satisfied $e^{K_{1m}t} > 0 \Rightarrow |e^{K_{1m}t}| = e^{K_{1m}t}, \forall t \ge 0$. Using this condition and the bounds $\lambda_i \le \bar{\lambda}_i$, we can re-write (26) as:

$$\begin{aligned} &\tilde{I}_{dlc}(t) \le I_{th} \triangleq \tilde{I}_{dlc}(0)e^{K_{1m}t} + \\ &\int_0^t \{e^{K_{1m}(t-\tau)}\bar{\lambda}_1|I_{dlc}(\tau)| + e^{K_{1m}(t-\tau)}\bar{\lambda}_2|u(\tau)| \\ &+ e^{K_{1m}(t-\tau)}\bar{\lambda}_3|T(\tau)| + e^{K_{1m}(t-\tau)}\bar{\lambda}_4\}d\tau \end{aligned} \tag{27}$$

The equation (27) can be equivalently written as a dynamic system with the following state-space form:

$$\begin{aligned} \dot{x}_1 &= K_{1m}x_1 + \bar{\lambda}_1|I_{dlc}| \\ \dot{x}_2 &= K_{1m}x_2 + \bar{\lambda}_2|u| \\ \dot{x}_3 &= K_{1m}x_3 + \bar{\lambda}_3|T| \\ \dot{x}_4 &= K_{1m}x_4 + \bar{\lambda}_4 \\ I_{th} &= \tilde{I}_{dlc}(0)e^{K_{1m}t} + x_1 + x_2 + x_3 + x_4 \end{aligned} \tag{28}$$

where $\bar{\lambda}_i$, $|I_{dlc}|$, $|u|$, $|T|$ are the known inputs to the system, x_i are the internal states and I_{th} is the output of the system which is also the adaptive threshold to the $Residual\ 1$ which is $\tilde{I}_{dlc}$ in case of no fault.

Similar to the electrical observer error dynamics, the temperature observer error dynamics with additive uncertainties can be written as:

$$mc\dot{\tilde{T}} = -hA\tilde{T} - L_T\tilde{T} + \eta_T \tag{29}$$

where η_T is the uncertainty and possibly nonlinear function of states and inputs. The uncertainty can be approximated as a linearly parameterized function of measured signals affecting the thermal dynamics:

$$\eta_T \cong \vartheta_1 I_{dlc} + \vartheta_2 T + \vartheta_3 \tag{30}$$

where ϑ_i are generally time-varying, unknown but bounded coefficients and ϑ_3 captures all the nonlinearities and approximation errors of the linear parameterization. The known bounds of these parameters are $\vartheta_i \le \bar{\vartheta}_i$. Following the similar steps as in case of the electrical error dynamics, we can design the following state-space system:

$$\begin{aligned} \dot{z}_1 &= -(hA + L_T)z_1 + \bar{\vartheta}_1|I_{dlc}| \\ \dot{z}_2 &= -(hA + L_T)z_2 + \bar{\vartheta}_2|T| \\ \dot{z}_3 &= -(hA + L_T)z_3 + \bar{\vartheta}_3 \\ T_{th} &= \tilde{T}_{dlc}(0)e^{-(hA+L_T)t} + z_1 + z_2 + z_3 \end{aligned} \tag{31}$$

where $\bar{\vartheta}_i$, $|I_{dlc}|$, $|T|$ are the known inputs to the system, z_i are the internal states and T_{th} is the output of the system

which is also the adaptive threshold to the $Residual\ 2$.

IV. Simulation Studies

In this section, we present the simulation case studies to validate the effectiveness of the proposed diagnostic scheme. The model parameters of a commercial DLC have been adopted from [17]. The experimentally validated model of DLC is subjected to a cyclic current profile generally used as testing protocol [17]: The DLC is charged with 60 A until it reaches 3 V, then 15 sec rest period, then the DLC is discharged with 60 A until it reaches 1.5 V followed by another 15 sec of rest. The current profile along with the voltage and temperature responses are shown in Fig. 3 for a nominal (non-faulty) condition.

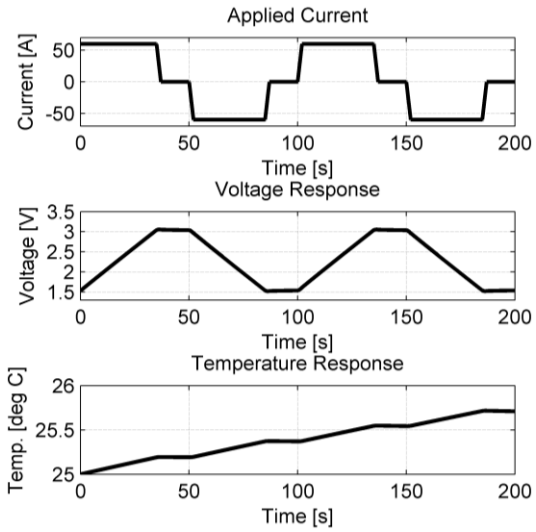

Figure 3: DLC current profile long with temperature and voltage responses

Based on the model parameters, the electrical observer gains are designed as a function of operating temperature and shown in Fig. 4. The temperature observer gain is chosen as constant 0.001.

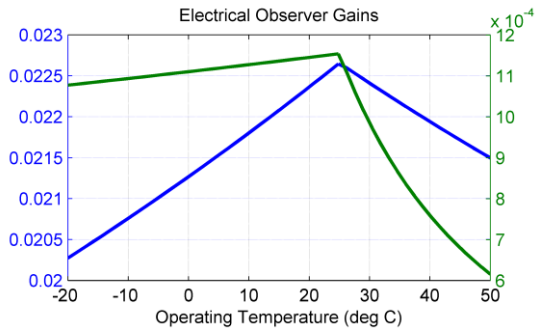

Figure 4: Electrical observer gains as functions of operating temperature

The isolability condition can be seen on the steady-state values of $Residual\ 1$ as a function of temperature sensor fault magnitude (Fig. 5). It can be seen that the effect of temperature sensor fault is relatively small on this residual and may not be visible in presence of uncertainties and measurement noise.

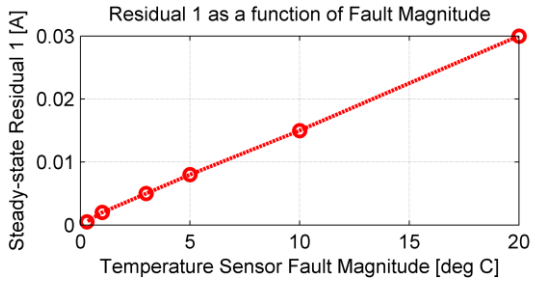

Figure 5: Steady-state values of *Residual 1* as a function of temperature senor fault magnitude.

Next, we test the effectiveness of the proposed approach. To emulate a realistic scenario, we inject measurement noise of 0.05 V, 0.1 deg C and 0.2 A and modeling uncertainties as shown in (24) and (30). We simulate four test scenarios.

Test Case 1: A voltage bias fault of 0.4 V is injected at 150 sec and the residual responses are given in Fig. 6. Note that, as shown in Table 1, the residual shows the signature $Residual\ 1 = 1$, $Residual\ 2 = 0$ confirming it to be a voltage sensor fault. As the fault under consideration is a bias fault, we are able to see a spike at 150 sec.

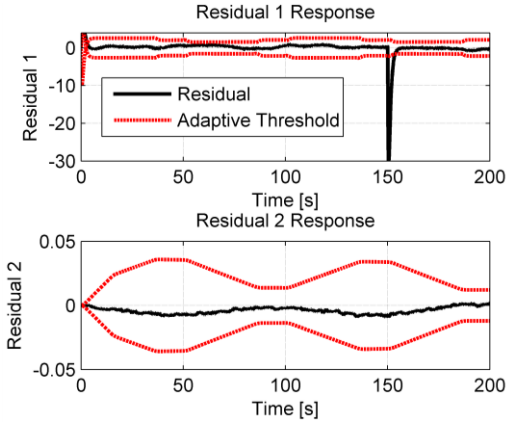

Figure 6: Residual responses for Test case 1 (voltage sensor bias fault 0.4 V injected at 150 sec)

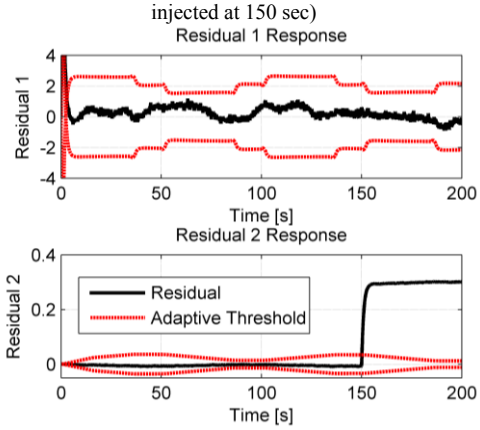

Figure 7: Residual responses for Test case 2 (temperature sensor bias fault 0.3 deg C injected at 150 sec)

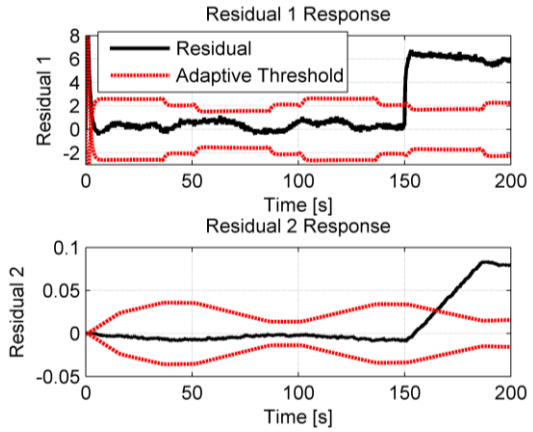

Figure 8: Residual responses for Test case 3 (current sensor bias fault 10 A injected at 150 sec)

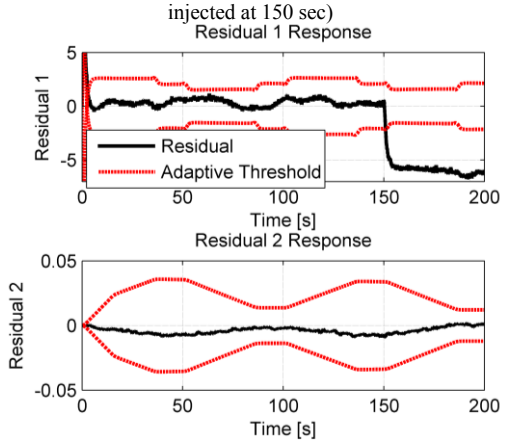

Figure 9: Residual responses for Test case 4 (voltage sensor incipient ramp-type fault 0.02 V/sec injected at 150 sec)

Test Case 2: A temperature bias fault of 0.3 deg C is injected at 150 sec and the residual responses are given in Fig. 7. Note that, as shown in Table 1, the residual shows the signature $Residual\ 1 = 0$, $Residual\ 2 = 1$ confirming it to be a temperature sensor fault. As the fault magnitude is not too large, therefore, this fault is isolable from the current sensor fault.

Test Case 3: A current sensor bias fault of 10 A is injected at 150 sec and the residual responses are given in Fig. 8. In this case, both of the residuals are high confirming it to be a current sensor fault.

Test Case 4: An incipient voltage sensor fault with a 0.02V/sec rate is injected at 150 sec and the residual responses are given in Fig. 9. In this case, $Residual\ 1$ settles to a constant value above the threshold as the fault is of ramp-type whereas $Residual\ 2$ remains below the threshold.

V. Conclusion

In this paper a model-based sensor fault diagnosis approach is presented for DLCs. The diagnostic scheme is based on two observers, electrical observer and temperature observer. The output errors of these observers are used as residuals for fault detection. To suppress the effect of modeling uncertainties, adaptive threshold generators have been designed.. The future extension of this work will be the experimental validation of the scheme under different operating conditions.

References

[1] P. Thounthong, S. Rael, and B. Davat, "Energy Management of Fuel Cell/Battery/Supercapacitor Hybrid Power Source for Vehicle Application," in *Journal of Power Sources*, vol. 193, no. 1, pp. 376-385, 2009.

[2] M. Marracci, B. Tellini, M. Catelani, and L. Ciani, "Ultracapacitor Degradation State Diagnosis via Electrochemical Impedance Spectroscopy," in *IEEE Trans. On Instrumentation and Measurement*, vol. 64, no. 7, pp. 1916-1921, 2015.

[3] C. Chiang, J. Yang, and W. Cheng, "EKF-based Estimation of SOC and Temperature in Ultracapacitors," in *IEEE International Conference on Control and Automation*, pp. 274-279, 2013.

[4] O. Bohlen, J. Kowal, and D. U. Sauer, "Ageing behaviour of electrochemical double layer capacitors: Part II. Lifetime simulation model for dynamic applications," in *Journal of Power Sources*, vol. 173, pp. 626-632, 2007.

[5] D. Pavkovic, V. Smetko, M. Hrgetic, and A. Komljenovic, "Dual Kalman filter-based SoC/SoH estimator for an ultracapacitor module," in *IEEE Control Applications*, pp. 1783-1788, 2014.

[6] A. Hammar, P. Venet, R. Lallemand, G. Coquery, and G. Rojat, "Study of accelerated aging of supercapacitors for transport applications," in *IEEE Transactions on Industrial Electronics*, vol. 57, no. 12, pp. 3972-3979, 2010.

[7] A. Nadeau, G. Sharma, and T. Soyata, "State-of-charge estimation for supercapacitors: a Kalman filtering formulation," in *IEEE International Conference on Acoustic, Speech and Signal Processing*, 2014.

[8] M. Pucci, G. Vitale, G. Cirrincione, and M. Cirrincione, "Parameter identification of a Double-Layer-Capacitor 2-branch model by a least-squares method," in *IEEE IECON*, pp. 6770-6776, 2013.

[9] A. Eddahech, O. Briat, M. Ayadi, and J. Vinassa, "Ultracapacitor performance determination using dynamic model parameter identification," in *IEEE International Symposium on Industrial Electronics*, pp. 1-5, 2013.

[10] S. Dey, S. Mohon, P. Pisu, B. Ayalew, S. Onori, "Online State and Parameter Estimation of Battery-Double Layer Capacitor Hybrid Energy Storage System," in *IEEE Conference on Decision and Control*, pp. 676-681, 2015.

[11] T. Wei, S. Wang, X. Gao, "Deterioration Diagnosis of Ultracapacitor for Power Electronics Applications," in *International Conference on Sustainable Power Generation and Supply SUPERGEN*, 2009.

[12] J. Li, G. Wang, L. Wu, X. Li, "On-line fault-diagnosis study: Model-based fault diagnosis for ultracapacitors," in *IEEE Prognostics and System Health Management Conference*, pp. 158-162, 2014.

[13] A. Oukour, N. Omar, H. Gualous, A. Rachid, P. Van Den Bossche, J. Van Mierlo, "Electrical double-layer capacitors diagnosis using least square estimation method," in *Electric Power Systems Research*, vol. 117, pp. 69-75, 2014.

[14] M. Marracci, B. Tellini, M. Catelani, L. Ciani, "Ultracapacitor degradation state diagnosis via electrochemical impedance spectroscopy," in *IEEE Transactions on Instrumentation and Measurement*, vol. 64, no. 7, pp. 1916-1921, 2015.

[15] Gertler, Janos. *Fault Detection and Diagnosis in Engineering Systems*. CRC press, 1998.

[16] Zhang, Xiaodong, Marios M. Polycarpou, and Thomas Parisini. "A robust detection and isolation scheme for abrupt and incipient faults in nonlinear systems." *IEEE Transactions on Automatic Control*, vol. 47, no. 4, pp. 576-593, 2002.

[17] S. Fiorenti, J. Guanetti, Y. Guezennec, and S. Onori, "Modeling and experimental validation of a hybridized energy storage system for automotive applications," in *Journal of Power Sources,* pp. 112-120, 2013.

[18] P. Ioannou, and J. Sun, *Robust Adaptive Control*. Englewood Cliffs, NJ: Prentice-Hall, 1996.

[19] Maxwell BCAP1500 data-sheet. Maxwell Technologies Official Website (2012).